International Journal of Thermal Sciences 48 (2009) 1049–1059

Contents lists available at ScienceDirect

International Journal of Thermal Sciences

www.elsevier.com/locate/ijts

Boiling heat transfer in vertical minichannels. Liquid crystal experiments and numerical investigations

Sylwia Hozejowska [a], Magdalena Piasecka [a], Mieczyslaw E. Poniewski [b,*]

[a] Kielce University of Technology, Al. 1000-lecia P.P 7, 25-314 Kielce, Poland
[b] Warsaw University of Technology, Plock Campus, Jachowicza 2/4, 04-101 Plock, Poland

ARTICLE INFO

Article history:
Received 11 October 2007
Received in revised form 14 November 2008
Accepted 17 November 2008
Available online 20 December 2008

Keywords:
Flow boiling incipience
Heat polynomials
Inverse boundary problem
Liquid crystals
Minichannel

ABSTRACT

The paper presents the results of experimental and numerical studies of boiling heat transfer in the flow of refrigerants R123 and R11 through vertical, rectangular minichannels, with one wall heated. An application of liquid crystal thermography has helped detect two-dimensional temperature distribution on the heating surface, allowing determination of boiling heat fluxes and experimental boiling curves. The main objectives of the paper included the development of two-dimensional approach to solve the inverse heat conduction boundary problem for determining local values of internal heating surface temperature, boiling heat flux and heat transfer coefficient, and the improvement of the applied numerical method making use of the equalizing calculus and heating surface temperature measurement errors. A detailed discussion of temperature, heat flux and heat transfer coefficient errors is also provided.

1. Literature review

Huge number of high-tech heat exchange devices including electronic instruments, high heat flux laser diodes, heat pipes, internal combustion engines, etc., use the phenomenon of heat transfer to boiling liquids flowing in minichannels of various geometry. Despite the growing number of new works dealing with flow boiling heat transfer in minichannels of various geometries, the results refer mainly to a narrow variation range of flow boiling parameters.

The effect of minichannel size on the flow boiling heat transfer coefficient, the onset of nucleate boiling and critical heat flux are discussed in the following papers [1,11,21,22,24,25,33,35,39,42,44]. In the majority of the quoted works, the flow boiling heat transfer coefficient significantly increases with reduced size of a minichannel [1,21,22,24,25,35,39,44]. Most of the reviewed papers [25,33,41, 42] have found no apparent effect of the inlet liquid subcooling on nucleate boiling. In works [6,21] the flow boiling heat transfer coefficient increased with the subcooling increase. The subcooling increase also brought about the heat flux increase required for nucleate boiling incipience [7,29,31]. The system pressure has appeared to have no clear effect on nucleate boiling incipience [7, 12,26,30,31,35]. It strongly influences the flow boiling heat transfer coefficient, which increases with the pressure growth [2,20,22, 40,43]. Nucleate boiling incipience depends quite clearly on the minichannel size [24,25,33,39,41], mass flux [7,12,45] and inlet liquid subcooling [7,21]. The increase in mass flux [7] and inlet liquid subcooling [7,21] caused the increase in the heat flux needed for boiling incipience. The nucleate boiling incipience wall superheat went down when the mass flux went up [12,45]. In most of the examined papers the flow boiling heat transfer coefficient has been fairly independent of the flow velocity or mass flux [2,22,23,25,27, 30,34,41,45]. Almost all the experiments show that the flow boiling heat transfer coefficient rises with the imposed heat flux [2,20, 22,23,34,40,43].

In the minichannels, incipience of boiling of a liquid with a small wetting angle (the refrigerants investigated) is frequently accompanied by nucleation hysteresis, together with a considerable heating surface temperature drop [6,7,12,14,15,19,26,27,30,31,45]. Hollingsworth in [14,15] proposed a parameter, described as "turning angle", to denote the boiling incipience as dependent on the course of nucleation hysteresis.

The three exhaustive, critical and different reviews by Kandlikar [18], Tadrist [37] and Thome [38] present current knowledge of the boiling heat transfer in minichannels in many aspects, including boiling incipience phenomenon accompanied with nucleation hysteresis, the impact of selected parameters on boiling heat transfer in minichannels and numerical methods to solve the inverse boundary problem. The impact of the discussed parameters, as our literature review shows, is not consistent and demands further experimental investigations and theoretical analysis.

The main raw data available in minichannel boiling heat transfer experiment applying thermosensitive liquid crystal technique is the hue distribution along the heating foil and the volumetric heat

* Corresponding author.
E-mail addresses: ztpsf@tu.kielce.pl (S. Hozejowska), tmpmj@tu.kielce.pl (M. Piasecka), meponiewski@pw.plock.pl (M.E. Poniewski).

1290-0729/$ – see front matter
doi:10.1016/j.ijthermalsci.2008.11.013

Nomenclature

a_i, b_i	coefficient	
BI	boiling incipience	
G	mass flux	$kg\,m^{-2}\,s^{-1}$
H	depth	m
H, S, I	hue, saturation and intensity components	
hue_k	hue value corresponding to the set foil temperature	
I	current	A
J	error functional	
L	length	m
M	number of heat polynomials number of hue images	
N	number of heat polynomials	
n	degree of a polynomial normal coordinate	m
p	pressure	$N\,m^{-2}$
R, G, B	red, green and blue components	
R^2	determination coefficient	
Q_V	volumetric flow rate	$m^3\,s^{-1}$
q_w	heat flux	$W\,m^{-2}$
q_V	volumetric heat flux (capacity of internal heat source)	$W\,m^{-3}$
s	variable of integration	
SEE	standard error estimation	
T	temperature	K
u_n	heat polynomial	
U	voltage drop	V
W	width	m
x	coordinate; distance along the channel length	m
y	coordinate; distance along the glass and foil thickness	m

Greek letters

α	heat transfer coefficient	$W\,m^{-2}\,K^{-1}$
Γ	boundary of domain of integration	
γ	arbitrary function	
Δ	absolute error (accuracy)	
ΔT_{sat}	surface superheating, $T_F - T_{sat}$	K
ΔT_{sub}	inlet liquid subcooling, $(T_{sat} - T_l)_{inlet}$	K
δ	thickness	m
ε_κ	temperature measurement correction	K
σ	mean temperature error	K
σ_k	temperature measurement error	K
ψ	arbitrary function	
Ω	Lagrange function domain of integration	
ω_n	Lagrange multiplier	

Subscripts

cal	calibration
card	card of the data acquisition station
ch	minichannel
F	foil
G	glass
k	measurement point
l	liquid
m	as measured
therm	thermocouple
1D, 2D	model dimension

Superscripts

$\sim$	refers to smoothed measurements

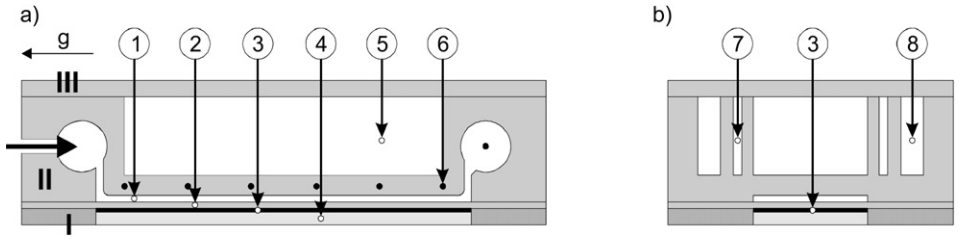

Fig. 1. Diagram of the test section with a minichannel: (a) vertical cross-section, (b) horizontal cross-section; I – front cover, II – main part with a minichannel and auxiliary channels, III – rear cover; #1 – minichannel, #2 – heating foil, #3 – thermosensitive liquid crystals, #4 – glass, #5 – auxiliary channel with flowing water of controlled temperature, #6 – back wall with thermocouples, #7 – air gap; #8 – auxiliary channel with flowing tap water to cool clamped edges of the foil.

flux, generated inside the foil. Local surface temperature, boiling heat flux and heat transfer coefficient can only be obtained from a relatively sophisticated data reduction procedure, which requires a solution to the inverse two-dimensional boundary heat conduction problem [6,26–28,32]. The heat polynomials method used here applies to both direct and inverse problems, it does not require high capacity computers, sophisticated software as or the conditions theoretically needed to solve a certain problem [9,17,27,28].

2. Experiment

2.1. Test section

The test section, Fig. 1, contains a vertical, rectangular minichannel of the following depths: 0.7; 1; 1.5 and 2 mm, widths: 20 mm or 40 mm and length 360 mm, with a refrigerant (R11, R123) flowing through it. The heating foil (0.1 mm thick, made of Haynes 230 alloy of high electrical and thermal resistivity) supplied with the direct current of controlled rate makes one of the channel walls. A layer of thermosensitive liquid crystals (Hallcrest) is deposited on the external foil surface, on a black base paint. Changes in the foil surface hue can be observed through an opening covered with a glass pane.

Auxiliary channels in the test section rear cover help to maintain the required temperature at constant level across the minichannel width and the longitudinal temperature distribution on its back wall, which is considered to be quasi-adiabatic. The idea of the experimental stand scheme was based on Chin and Hollingsworth publications [6,7,14] with certain modifications related to all elements of the entire system [26,27,29,30].

2.2. The flow loop and the systems of data acquisition and processing

The main loop of the flow system for the boiling process examination consists of the following elements (Fig. 2): vertical test

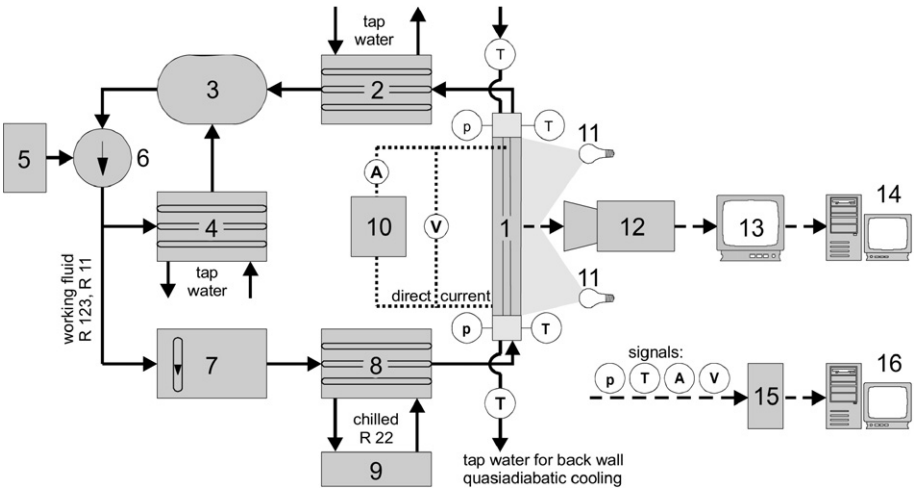

Fig. 2. Block diagram with main elements: #1 – vertical test section with a minichannel, #2, #4, #8 – plate type heat exchangers, #3 – compensating tank, #5 – frequency inverter, #6 – rotary pump, #7 – flow meters, #9 – recirculation cooler, #10 – direct current power supply, #11 – fluorescent lamps, #12 – CCD video camera with RGB signal decomposer, #13 – video recorder with monitor, #14 – computer with frame grabber, #15 – data acquisition station, #16 – computer; A – ammeter; p – pressure transducer; T – type K thermocouple; V – voltmeter.

section with minichannel (#1); heat exchangers (#2, #4, #8); compensating tank (#3); frequency inverter (#5) that changes the rotational speed of the pump rotor to control the flow rate and prevents cavitations in the pump; rotary pump (#6); flow meters (#7). The set-up is supplemented with recirculation cooler (#9), direct current power supply (#10), and pressure, temperature, current and voltage drop meters.

A complex system for data and color images acquisition and processing, presented in Fig. 2, consists of: a lighting module (#11), which has two sources of white "cold" light, located at the same distance from the investigated object and at the same angle to it; a CCD video camera with an RGB signal decomposer (#12), located at the front of investigated object; video recorder with monitor (#13) and PC with frame grabber (#14). Software for the acquisition card and software for measurement data processing supplement the image acquisition system. Temperature and pressure control and acquisition in various parts of the test section are performed by a data acquisition station (#15) together with appropriate software installed on another computer (#16).

2.3. What are we trying to find

The system under investigation, Fig. 3, consists of the working liquid (R123, R11) and two vertical walls: a quasi-adiabatic wall on one side (Fig. 1, #7; Fig. 3) and the heating foil (Fig. 1, #2; Fig. 3) with glass (Fig. 1, #4; Fig. 3) on the other. The liquid, at the temperature below its boiling point, flows into the minichannel (Fig. 1, #1, Fig. 3). Gradual increase in the electric power supplied to the foil results in an increased heat flux transferred to the flowing liquid in the minichannel. This leads to the incipience and then to the development of nucleate boiling. Owing to the liquid crystal layer located on its surface contacting the glass, it is possible to measure temperature distribution on the heating wall.

Wanted values include local temperature, local heat flux and finally local heat transfer coefficient on the foil internal surface in contact with the boiling liquid. This is an inverse boundary problem. It is possible to determine the unknown boundary conditions on the basis of temperature measurement at the system internal points (temperature distribution on the heating foil on the side of the glass) and the measurement of the electric power supplied to the heater [6,27,28,32]. Steady state conditions were assumed for the entire system, whereas the thickness of liquid crystal layers and temperature changes of glass, foil and liquid along the minichannel width were omitted.

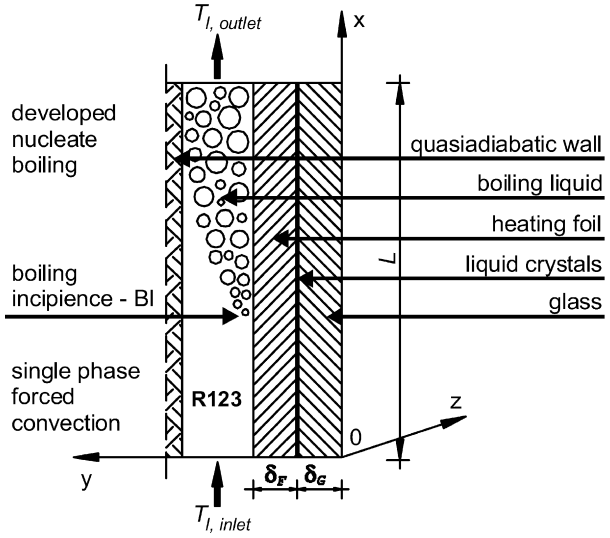

Fig. 3. Diagram of the flow boiling process in the investigated minichannel.

Color image acquisition system based on three basic colors R, G and B was used in the investigations. When the liquid crystals calibration and the measurements take place in identical and constant geometrical and lighting conditions, the HSI system allows conversion of three-component RGB signal into a single hue matrix [13,26]. RGB components of the color image of any pixel of the observed surface with variable temperature recorded by the measurement system, Fig. 4a, are converted to a hue scalar value in accordance with the following equation:

$$hue = \arctan\left(\frac{\sqrt{3}(G-B)}{2R-G-B}\right) \tag{1}$$

Application of liquid crystals to the detection of two-dimensional heating surface temperature distribution must be preceded by hue–temperature calibration. As a result of the calibration the curve temperature = function(hue) is obtained, Fig. 4b [26,28–30]. Details of the calibration procedure can be found in [6,13,26].

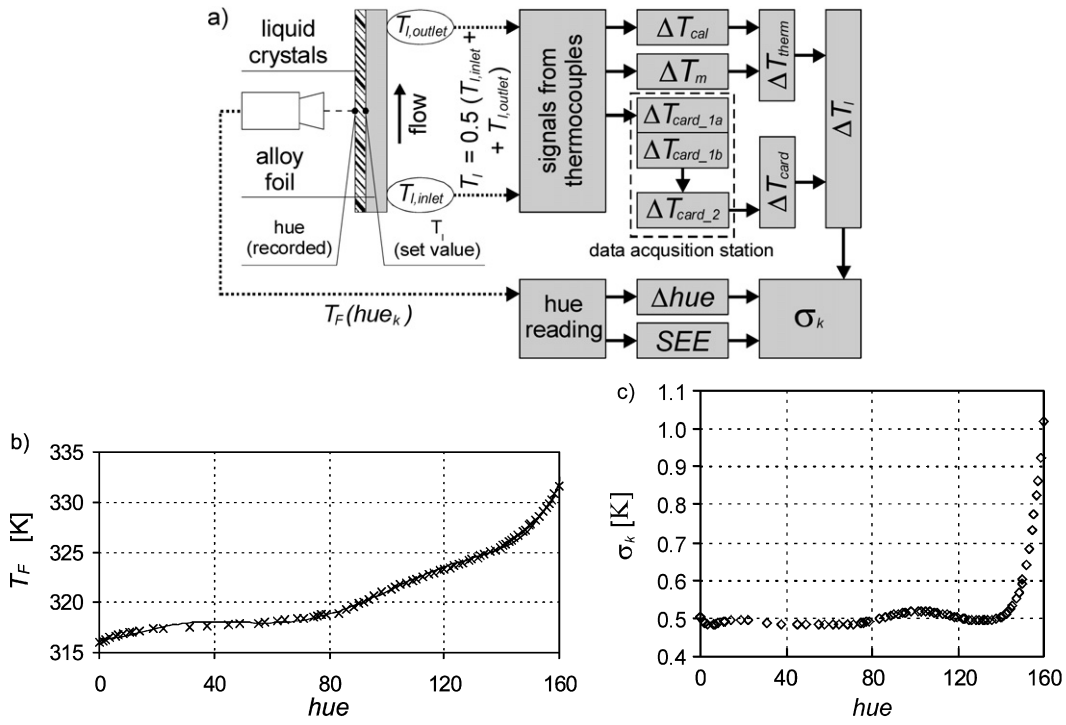

Fig. 4. (a) Diagram of measurement data acquisition system with marked error generation sites; (b) calibration curve; (c) graph of dependence of temperature error as a function of hue $T_F = 7.93\text{E}{-}11hue^6 - 3.6\text{E}{-}08hue^5 + 6.05\text{E}{-}06hue^4 - 4.52\text{E}{-}04hue^3 + 1.43\text{E}{-}02hue^2 - 1.11\text{E}{-}01hue + 17\text{E}{+}02$, $R^2 = 0.995$.

2.4. Assessment of accuracy of selected parameters

The measurement error of the external foil surface temperature generates an error in the calculation of local temperature of the foil contacting the boiling liquid T_F, heat flux q_w and heat transfer coefficient α. They are discussed in Section 3. Temperature measurements errors were used to modify the applied numerical methods, Section 4.

2.4.1. Foil temperature

The mean square error was assumed as a measure of an error magnitude [16]. Mean square errors were computed as roots of the sum of squares of products of the function partial derivatives by the given parameter measurement mean error. The derivatives were taken with respect to external parameters occurring in direct measurements. The diagram with marked areas of error generation in the course of experiments is shown in Fig. 4a.

It is assumed that, similar to [13], the mean temperature error for a single point determined on the basis of hue in the calibration experiment, amounts to:

$$\sigma = \frac{1}{M}\sum_{k=1}^{M}\sigma_k = \frac{1}{M}\sum_{k=1}^{M}\sqrt{\left(\frac{\partial T_F(hue_k)}{\partial hue_k}\cdot \Delta hue\right)^2 + (2\cdot SEE)^2 + (\Delta T_l)^2} \tag{2}$$

SEE relates to the fitting of the calibration curve and it is determined with the least square method:

$$SEE = \sqrt{\frac{1}{M}\sum_{k=1}^{M}\left(T_F(hue_k) - T_l\right)^2 (M-n-1)^{-1}} \tag{3}$$

ΔT_l represents the overall liquid temperature errors at the minichannel inlet and outlet, which result from signal processing by acquisition cards and from errors in thermocouples:

$$\Delta T_l = \sqrt{(\Delta T_{\text{card}})^2 + (\Delta T_{\text{therm}})^2} \tag{4}$$

The error resulting from signal processing by the data acquisition station amounts to:

$$\Delta T_{\text{card}} = \sqrt{(\Delta T_{\text{card\_1}a})^2 + (\Delta T_{\text{card\_1}b})^2 + (\Delta T_{\text{card\_2}})^2} \tag{5}$$

where AIM7 (Keithley) thermocouple card errors ($\Delta T_{\text{card\_1}a}$, $\Delta T_{\text{card\_1}b}$, denoted as #5a and #5b in Fig. 4a.) and also an error of AMM2 (Keithley) card (16-bit analogue-digital converter – $\Delta T_{\text{card\_2}}$) should be accounted for.

The sensor error ΔT_{therm} results from errors in the thermocouple calibrating and in the direct measurement, leading the equation:

$$\Delta T_{\text{therm}} = \sqrt{(\Delta T_{\text{cal}})^2 + (\Delta T_m)^2} \tag{6}$$

Detailed values of all particular errors mentioned above, were given in [26,32].

After inserting appropriate numerical values into (7), mean temperature measurement error $\sigma = 0.86$ K is obtained [17,26,28]. An exemplary graph of temperature errors as a function of hue related to the calibration curve from Fig. 4b, is shown in Fig. 4c.

2.4.2. Volumetric heat flux

In order to calculate the volumetric heat flux error, an experiment at low electric power was conducted, generating volumetric heat flux $q_V = 1.02\cdot 10^8$ W/m^3, for a minichannel of 40 mm in width and 1 mm in depth. The volumetric heat flux was determined from the electric power supplied to the heating foil, Eq. (1), for which the mean square error is:

$$\Delta q_V = \left(\left(\frac{\partial q_V}{\partial I}\cdot \Delta I\right)^2 + \left(\frac{\partial q_V}{\partial U}\cdot \Delta U\right)^2 + \left(\frac{\partial q_V}{\partial L_F}\cdot \Delta L_F\right)^2 + \left(\frac{\partial q_V}{\partial W_F}\cdot \Delta W_F\right)^2 + \left(\frac{\partial q_V}{\partial \delta_F}\cdot \Delta \delta_F\right)^2\right)^{1/2} \tag{7}$$

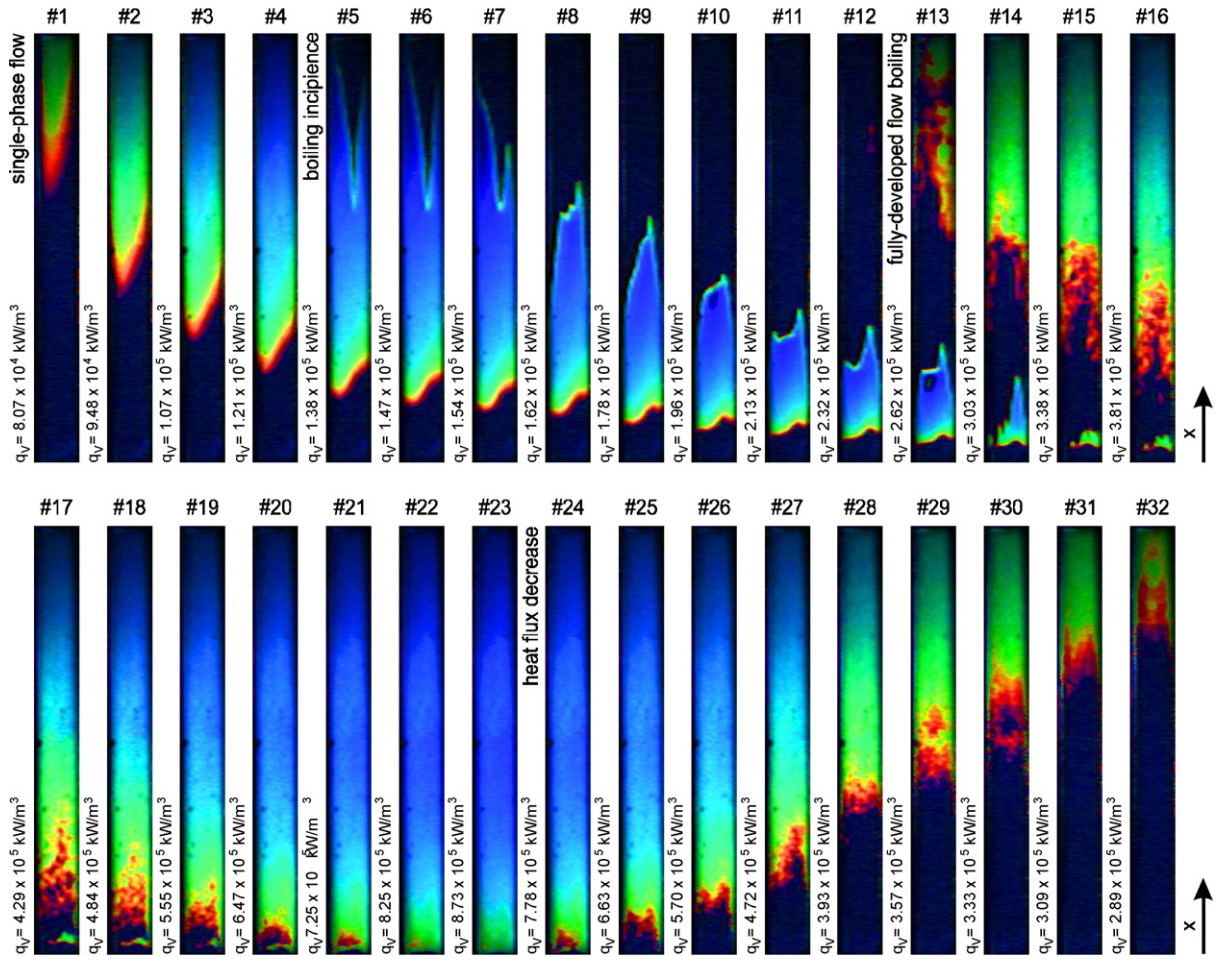

Fig. 5. Images of hue temperature distribution on the minichannel heating wall while initially increasing (from #1 up to #23) and then decreasing (from #24 up to #32) heat flux supplied to the heating surface; experimental parameters: R 123, $G = 412$ kg/m^2 s; $p_{\text{inlet}} = 0.19$ MPa; $\Delta T_{\text{sub}} = 36$ K; $q_V = 8.07 \cdot 10^4$–$8.73 \cdot 10^5$ kW/m^3, $q_w =$ 8.2–88.6 kW/m^2; $H_{\text{ch}} = 1$ mm, $W_{\text{ch}} = 40$ mm [26].

Absolute errors of particular measurements were defined on the basis of the accuracy of the measuring devices used and their details are given in [26].

Ultimately, the relative error of volumetric heat flux measurement in the considered case equals

$$\Delta q_V / q_V \cdot 100\% = 2.04\% \tag{8}$$

which was assumed a satisfactory result.

2.4.3. Other parameters and the boundary conditions

Mean square errors of other measured parameters were estimated in the following way [26]: inlet (outlet) liquid temperature $\Delta T_{l,\text{inlet}} \approx 0.39$ K, inlet liquid subcooling $\Delta(\Delta T_{\text{sub}}) \approx 0.68$ K, inlet (outlet) pressure $\Delta p_{\text{inlet}} \approx 0.7$ kPa and volumetric flow rate $\Delta Q_V \approx 1.7\%$.

Quasi-adiabatic boundary condition on the minichannel back wall, Fig. 1, is obtained through appropriate adjustment of water flow from the tap and the resulting average temperature of the wall. This temperature is maintained close to an average value of the inlet and outlet temperatures of the flowing liquid with an error less than ± 1 K throughout the entire experiment. Therefore, almost net zero temperature difference is maintained across the back surface.

In order to estimate heat losses to the environment through the glass pane, Fig. 1, the experimental stand was equipped temporarily with an infrared thermovision camera, placed immediately behind the CCD camera, Fig. 3, to measure temperature on the glass external surface [29]. Computations of local boiling heat transfer coefficients, keeping in view heat losses to the environment, show that their impact can be disregarded since they could lower the coefficient value by 2% at the most [29].

2.5. Experimental procedure and results

Raw data are obtained as sets of hue distribution images on the heating surface coated with liquid crystals, Fig. 5.

During the first increase of power q_V, the heat transfer between the foil and the liquid proceeds by single-phase forced convection, Fig. 5 – images #1 to #4. It is manifested in the form of subsequent hues in the visible spectrum sequence and shows gradual increase in the heating surface temperature (black color on the surface indicates that the surface temperature is beyond the liquid crystal sensitivity range).

When q_V is increased continuously as in Fig. 5 – images #5 to #14, occurrence of the "boiling front" (*BI*) is seen as rapid hue changes on the foil, taking place inversely to the spectrum sequence, then the black hue returns (mostly in lower parts of the images). This indicates sudden heating foil temperature drop. *BI* is identified with the maximum heating surface temperature, Fig. 6. The abrupt decrease in heating surface temperature results from the vapor bubbles spontaneous formation in the wall adjacent layer. They function as internal heat sinks, absorbing significant amount of energy transferred to the liquid [3,4,26,27,30]. This phenomenon has been discussed in detail in [6,15,27].

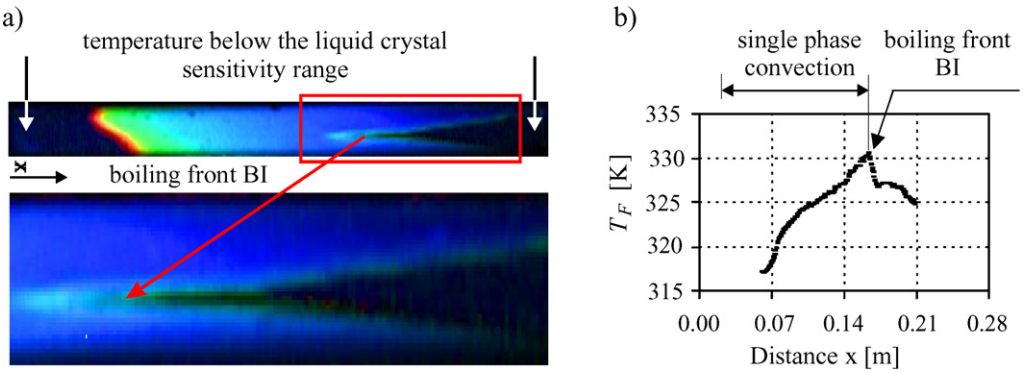

Fig. 6. (a) Selected enlarged image of hue distribution along the heating foil (Fig. 5, #5) and the enlarged picture of the "boiling front" area; (b) foil temperature dependence on the distance along the channel length equivalent to the chosen hue image, Fig. 6a [26].

When the heat flux is being increased further, Fig. 5 – images from #14 on, black hue is replaced with a new hue sequence, mostly in the upper part of images. This occurs when developed nucleate boiling is in progress in the channel. From the point where saturated navy blue hue appeared on the foil surface, Fig. 5 – image #23, the current supplied to the foil is gradually decreased.

This causes mild hue change in the direction opposite to the spectrum sequence. As a result, heat transfer returns to forced single-phase convection. Gradual decrease in the heat flux makes the boiling process disappear first at the channel inlet, and boiling "fading away" moves downstream, Fig. 5 – images #24 to #32. At the end of the run, black hue returns covering the entire heating foil area and this indicates that the temperature has dropped below the liquid crystal active range.

3. Flow boiling heat transfer numerical calculations

The raw data in the presented experiments are as follows: liquid crystal hue distribution on the heating foil, volumetric heat flux (capacity of the internal heat source), inlet and outlet temperatures of the boiling liquid and the volumetric flow rate. As already mentioned, the liquid crystal data have to be reduced with the application of the solution to the inverse heat conduction problem [6,26–28]. This allows us to obtain the sought-after local parameters on the foil surface contacting the boiling liquid, Fig. 7, that is, the foil temperature $T_F(x, \delta_G + \delta_F)$, the heat flux $q_w(x, \delta_G + \delta_F)$ and the heat transfer coefficient $\alpha(x)$.

3.1. Two-dimensional approach

A careful examination of liquid crystal images of the foil external surface temperature, Fig. 5, allow us to assume that at a small distance from the boiling point the foil temperature is almost constant along the foil width, that is, along coordinate z, Fig. 3. This is due to the application of auxiliary cooling channels with flowing tap water, Fig. 1, #8. The observation leads us to the conclusion that the two-dimensional model of heat transfer along the coordinates x (test section length) and y (thickness), Fig. 3, is suitable enough for the investigated case.

A stationary heat conduction process in a two-layer partition (the foil and the glass) is expressed with the equations:

(a) in the glass

$$\nabla^2 T_G = 0 \tag{9}$$

(b) in the foil

$$\nabla^2 T_F = -\frac{q_V}{\lambda_F} \tag{10}$$

$$q_V = \frac{U \cdot I}{\delta_F \cdot W_F \cdot L_F} \tag{11}$$

At the glass–foil contact the equality of both temperatures and their gradients (heat fluxes) is required, Fig. 7:

$$T_F(x_k, \delta_G) = T_G(x_k, \delta_G) = T_k \quad \text{for } k = 1, 2, \ldots, K \tag{12}$$

$$\lambda_F \frac{\partial T_F}{\partial y} = \lambda_G \frac{\partial T_G}{\partial y} \quad \text{for } y = \delta_G \text{ and } 0 \leqslant x \leqslant L \tag{13}$$

where: T_k denotes the measurement temperature read with liquid crystal thermography technique at the measurement points (x_k, δ_G) in boiling experiments.

It is assumed that the remaining boundaries at $x = 0, x = L$ and $y = 0$ are insulated, Fig. 7.

On the heating foil surface contacting the flowing liquid, for $y = \delta_G + \delta_F$, the unknown boundary condition is expressed in the following way:

$$-\lambda_F \frac{\partial T_F(x, \delta_G + \delta_F)}{\partial y} = \alpha_{2D}(x)\big(T_F(x, \delta_G + \delta_F) - T_l(x)\big) \tag{14}$$

Eq. (14) contains two unknown functions: temperature $T_F(x, \delta_G + \delta_F)$ and the heat transfer coefficient α_{2D}. Local bulk liquid temperature T_l is calculated on the basis of the enthalpy balance [26,27, 31,32].

The problem (9)–(13) was solved under the analytical–numerical heat polynomials method. The method allows simple solving of direct and inverse heat conduction problems, giving very small solution errors [9]. The method has been validated against known solutions obtained analytically or with the finite element method [8].

Heat polynomials $u_n(x, y)$, which satisfy Eq. (9), are used to find temperature $T_F(x, y)$ [9,27]. The unknown glass temperature $T_G(x, y)$ is approximated with a linear combination of the heat polynomials $u_n(x, y)$, whereas the foil temperature $T_F(x, y)$ is given as a sum of the function being a specific solution $\tilde{u}(x, y)$ to Eq. (10) and the linear combination of polynomials $u_n(x, y)$:

$$T_G(x, y) \approx \sum_{i=0}^{N} a_i u_i(x, y)$$

$$T_F(x, y) \approx \tilde{u}(x, y) + \sum_{j=0}^{M} b_j u_j(x, y) \tag{15}$$

Unknown coefficients a_i and b_j for $i = 0, 1, \ldots, N$, $j = 0, 1, \ldots, M$ are calculated by means of two techniques. One, using the least squares method, leads to the minimization of error functional, appropriate to each of the functions $T_G(x, y)$ and $T_F(x, y)$. Those functionals describe the mean squared error between approximates and prescribed boundary conditions. It is a heat polynomials method [9,28].

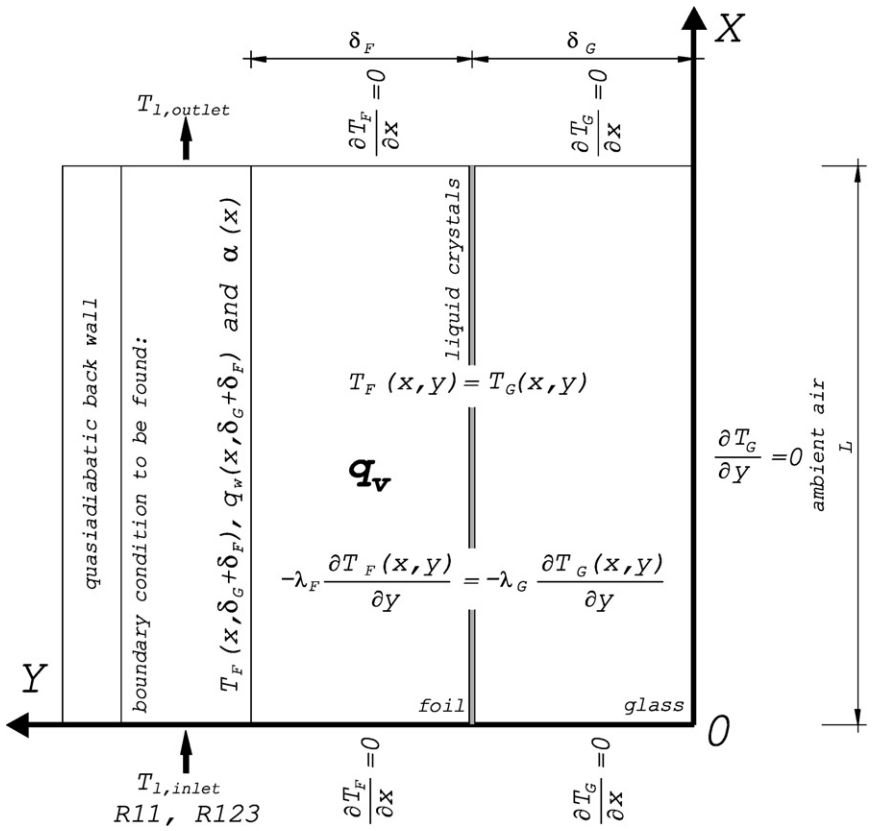

Fig. 7. Boundary conditions for a two-dimensional model.

For function $T_G(x, y)$ the error functional J_G is defined as follows [9,28]:

$$J_G = \int_0^L \left(\frac{\partial T_G(x,0)}{\partial y}\right)^2 dx + \int_0^\delta \left[\left(\frac{\partial T_G(0,y)}{\partial x}\right)^2 + \left(\frac{\partial T_G(L,y)}{\partial x}\right)^2\right] dy + \sum_{k=1}^{K} \left(T_G(x_k,\delta_G) - T_k\right)^2 \tag{16}$$

When in the relationship (16), $T_G(x, y)$ is substituted with dependence (15), the minimum of the functional J_G is determined from the solution for the system of equations:

$$\frac{\partial J_G}{\partial a_i} = 0 \quad \text{for } i = 0, 1, \ldots, N \tag{17}$$

Unknown coefficients b_j, Eq. (15), are determined in the same way. For function $T_F(x, y)$, the minimized functional takes the following form:

$$J_F = \int_{\delta_G}^{\delta_G+\delta_F} \left(\frac{\partial T_F(0,y)}{\partial x}\right)^2 dy + \int_{\delta_G}^{\delta_G+\delta_F} \left(\frac{\partial T_F(L,y)}{\partial x}\right)^2 dy + \int_0^L \left(\frac{\partial T_F(x,\delta_G)}{\partial y} - \frac{\lambda_G}{\lambda_F}\frac{\partial T_G(x,\delta_G)}{\partial y}\right)^2 dx + \sum_{k=1}^{K} \left(T_F(x_k,\delta_G) - T_k\right)^2, \tag{18}$$

which leads to the following system of equations

$$\frac{\partial J_F}{\partial b_j} = 0 \quad \text{for } j = 0, 1, \ldots, M \tag{19}$$

In the other method, further referred to as the Trefftz method [10, 27], the starting point is Green's second identity

$$\iint_\Omega \left(\gamma\nabla^2\psi - \psi\nabla^2\gamma\right) dx\,dy = -\int_\Gamma \left(\gamma\frac{\partial\psi}{\partial n} - \psi\frac{\partial\gamma}{\partial n}\right) ds \tag{20}$$

By insertion of: $\gamma = \sum_{i=0}^{N} a_i u_i(x, y)$ and $\psi = u_j(x, y)$ in (20), we obtain the following set of equations expressing unknown coefficients $a_1, \ldots, a_N$:

$$\sum_{i=1}^{N} a_i \left\{\int_0^L \left[u_i(x,0)\frac{\partial u_j(x,0)}{\partial y} + u_i(x,\delta_G)\frac{\partial u_j(x,\delta_G)}{\partial y}\right] dx + \int_0^{\delta_G} \left[u_i(L,y)\frac{\partial u_j(L,y)}{\partial x} - u_i(0,y)\frac{\partial u_j(0,y)}{\partial x}\right] dy\right\} = \int_0^L T_k \frac{\partial u_j(x,\delta_G)}{\partial y} dx \tag{21}$$

Constant a_0 is chosen so that the function T_G satisfies the condition (12):

$$a_0^k = T_k - T_G(x_k, \delta_G) \tag{22}$$

A set of equations expressing unknown coefficients $b_1, \ldots, b_M$ is obtained in the similar way.

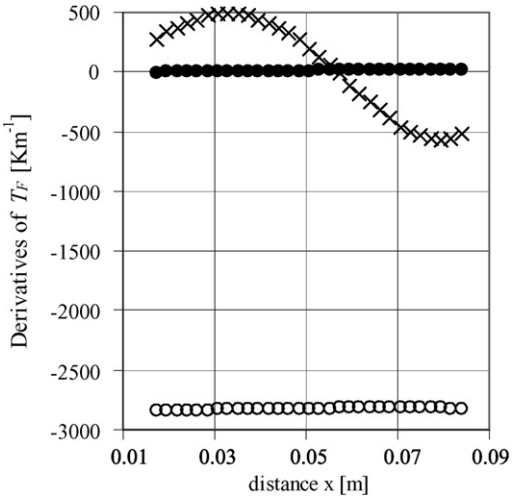

Fig. 8. First order derivates of the foil temperature: ∘ – $\partial T_F/\partial y|_{y=\delta_G+\delta_F}$, • – $\partial T_F/\partial y|_{y=\delta_G}$, × – $\partial T_F/\partial x|_{y=\delta_G+\delta_F}$ in a two-dimensional model for run #12.

In both two-dimensional methods, the approximation of the function $T_G(x, y)$ is computed first and then function $T_F(x, y)$ follows. Determining glass temperature $T_G(x, y)$ is a solution the direct problem given by Eq. (9) with boundary conditions presented in Fig. 7. The determination of foil temperature $T_F(x, y)$ – constitutes a solution to the discussed inverse heat conduction problem. Functions $T_G(x, y)$ and $T_F(x, y)$, so determined, satisfy both equations, (9) and (10), in an accurate way.

For heat polynomials, functions $T_G(x, y)$ and $T_F(x, y)$ satisfy conditions (12) and (13) approximately. In the Trefftz method, the functions named above meet approximately only condition (13); condition (12) is satisfied exactly. If we know the function $T_F(x, y)$ on the boundary $y = \delta_G + \delta_F$, we are able to calculate the heat flux going into flowing liquid, $q_w(x, \delta_G + \delta_F)$, and the heat transfer coefficient, $\alpha_{2D}(x)$, from condition (14).

3.2. One-dimensional approach

If simplified assumptions are made, the two-dimensional model shown above can be reduced to one-dimensional model. The glass pane, Fig. 7, owing to its very low conductivity ($\lambda_G = 0.71\ \mathrm{W\,m^{-1}\,K^{-1}}$), quite large thickness ($\delta_G = 5$ mm) and a low heat transfer coefficient on its external surface, may be treated as a perfect insulator. Therefore, it may be assumed that the entire volumetric heat flux generated inside the foil, is transferred by heat conduction across the foil thickness to the flowing liquid, and the heat flux on the surface contacting the liquid is given by the equation

$$-\lambda_F \frac{\partial T_F(x, \delta_G + \delta_F)}{\partial y} = q_V \delta_F = q_w \tag{23}$$

This assumption results from the fact that the derivative $|\partial T_F/\partial y|_{y=\delta_G+\delta_F}$ changes very little along the minichannel length and its values are much higher than values of derivatives $|\partial T_F/\partial x|_{y=\delta_G+\delta_F}$ and $|\partial T_F/\partial y|_{y=\delta_G}$, Fig. 8. This indicates that the largest heat flux generated inside the foil is passed to the boiling liquid in the direction normal to the heating surface.

With the foil thickness being very small ($\delta_F \cong 0.1$ mm), it is possible to replace the partial derivative in (23) with a finite difference:

$$\frac{\partial T_F(x, \delta_G + \delta_F)}{\partial y} = \frac{T_F(x, \delta_G + \delta_F) - T_F(x, \delta_G)}{\delta_F} \tag{24}$$

$T_F(x, \delta_G + \delta_F)$ is calculated from (23) and (24)

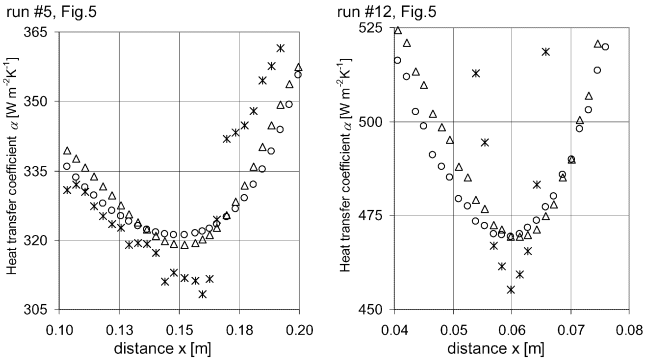

Fig. 9. Heat transfer coefficient in near boiling incipience: △ – α_{1D} (one-dimensional model), ∘ – $\alpha_{2D,1}$ (two-dimensional model and heat polynomials method), ∗ – $\alpha_{2D,2}$ (two-dimensional model and the Trefftz method).

$$T_F(x, \delta_G + \delta_F) = \frac{\lambda_F T_F(x, \delta_G) - q_V \delta_F^2}{\lambda_F} \tag{25}$$

Then, after taking conditions (14), (24) and (25) into account, we get a simple formula for the local heat transfer coefficient α_{1D}, [32]:

$$\alpha_{1D}(x) = \frac{q_V \cdot \lambda_F \cdot \delta_F}{\lambda_F (T_F(x, \delta_G) - T_l(x)) - q_V \cdot \delta_F^2} \tag{26}$$

In Eq. (26) $T_F(x_k, \delta_G)$ is obtained from approximation of the liquid crystal measurement results by an n-degree polynomial.

3.3. Results of calculations for one- and two-dimensional approaches

In the examples presented below, we provide the values of heat transfer coefficient versus distance x for the transition from single phase to boiling incipience. At first, $T_F(x, \delta_F + \delta_G)$ and the heat flux at the contact surface of the foil and liquid are calculated in the presented models. Then, the heat transfer coefficient α is calculated from formulae (14) and (26).

Thus, the formulae (14) and (26) accumulate all errors of measurements and calculations: foil temperature $T_F(x, \delta_G)$ measurement error, heat flux q_w calculation error and liquid temperature T_l estimation error. For this reason, in continuation of our research, we compare heat transfer coefficients for particular methods used in chosen experimental runs, shown in Fig. 5 as images of hue temperature distribution on the external surface of the heating foil.

It was assumed that for the two-dimensional approach $\tilde{u}(x, y) = -0.5 q_v \lambda_F^{-1} y^2$ and the number of approximating polynomials u_n: $N = M = 12$. In the one-dimensional approach liquid crystal temperature measurements T_k were approximated by a 5-degree polynomial: $n = 5$.

Fig. 9 presents the results obtained from the two-dimensional approach solved with the use of the two discussed methods, and the results obtained from one-dimensional approach. $\alpha_{2D,1}$ denotes heat transfer coefficient calculated from formula (14) after the heat polynomials method was used, $\alpha_{2D,2}$ – the coefficient calculated from (14) after the Trefftz method was used, α_{1D} – the coefficient calculated from (26).

Heat transfer coefficient $\alpha_{2D,2}$ (calculated with the use of the Trefftz method) differs in value when compared with the coefficients calculated with the use of other methods and its scatter is substantial. This is because the Trefftz method employs exact values of temperature T_k at the measuring points, whereas other methods smooth the data, either through the approximation with a polynomial (one-dimensional approach) or due to the heat polynomials method characteristics (two-dimensional approach). As the

Table 1
Mean errors of the heat flux q_w and of the heat transfer coefficient α for various calculation methods.

Method	Mean relative errors	
	Run #5 $q_V = 1.36 \cdot 10^5$ kW/m^3	Run #12 $q_V = 2.32 \cdot 10^5$ kW/m^3
Mean relative error $\Delta q_w/q_w$ (two-dimensional model, heat polynomials)	15.19%	16.35%
Mean relative error $\Delta q_w/q_w$ (two-dimensional model, Trefftz method)	29.45%	35.33%
Mean relative error $\Delta\alpha_{2D,1}/\alpha_{2D,1}$ (two-dimensional model, heat polynomials)	15.29%	16.45%
Mean relative error $\Delta\alpha_{2D,2}/\alpha_{2D,2}$ (two-dimensional model, Trefftz method)	29.57%	35.53%

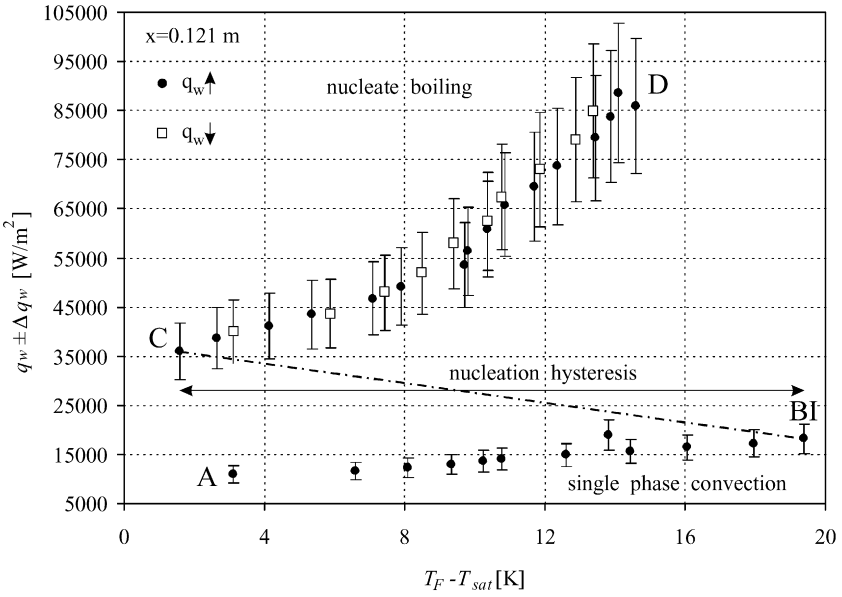

Fig. 10. Boiling curve at a distance of 0.121 m from the inlet; $q_w \pm \Delta q_w$ – heat flux and its error distributions; parameters as in Fig. 5 [26].

measurement data are not smoothed, the Trefftz method is more sensitive to measurement errors than other methods (see Table 1).

The error for q_w for the two-dimensional model was determined from the following formula:

$$\Delta q_w = \left[\left(\frac{\partial q_w}{\partial \lambda_F}\cdot\Delta\lambda_F\right)^2 + \left(\frac{\partial q_w}{\partial\frac{\partial T_F}{\partial y}}\cdot\Delta\frac{\partial T_F}{\partial y}\right)^2\right]^{1/2} \tag{27}$$

where: $\Delta\lambda_F = 0.01$ (W/m K); $\Delta\frac{\partial T_F}{\partial y} = |\frac{\partial^2 T_F}{\partial y^2}\Delta y|$ and Δy equals four times the pixel dimension ($\Delta y_{\text{pixel}} = 7.4 \cdot 10^{-4}$ m), as the measured temperature T_k is the average of temperature readings at the point and its four surrounding neighbors.

Heat transfer coefficient error $\Delta\alpha_{2D}$ is determined with the following formula

$$\Delta\alpha_{2D} = \left[\left(\frac{\partial\alpha_{2D}}{\partial T_F}\cdot\Delta T_F\right)^2 + \left(\frac{\partial\alpha_{2D}}{\partial T_l}\cdot\Delta T_l\right)^2 + \left(\frac{\partial\alpha_{2D}}{\partial q_w}\cdot\Delta q_w\right)^2\right]^{1/2} \tag{28}$$

where: $\Delta T_F(x_k, \delta_G) = \sigma_k$ (since the foil is very thin, we can assume that ΔT_F equals to the error of the temperature measurement); $\Delta T_l = 0.39$ K [26]; $\Delta q_w/q_w$ and $\Delta\alpha/\alpha$ denote the sought-after relative error.

Table 1 presents examples of mean errors of the q_w and of the heat transfer coefficient α for two-dimensional approaches. Mean errors were obtained as arithmetic mean of errors $\Delta q_w/q_w$ and $\Delta\alpha/\alpha$ determined at all possible measuring points x_k (the colorful part of the selected image, Fig. 5). The extent of error Δq_w is determined by derivative $\partial^2 T_F/\partial y^2$; the extent of error $\Delta\alpha$ is determined by error Δq_w. The Trefftz method is more sensitive (produces larger errors $\Delta\alpha$ and Δq_w, Table 1) to errors of data used in calculations, because the results are not smoothed the way they are in the heat polynomials method, Fig. 9.

Fig. 10 shows the exemplary boiling curve obtained on the basis of data already presented in Fig. 5. It is plotted as a function of the heat flux (on the surface contacting the flowing liquid) and surface superheating for the selected fixed distances from the minichannel inlet – $q_w = q_w(T_F - T_{\text{sat}})$. In accordance with results obtained earlier for one- and two-dimensional models presented in Fig. 9, a one-dimensional model was chosen for determining the boiling curve in Fig. 10. Detailed analysis of the boiling curves was presented earlier in [26,27,29,30].

4. Techniques to improve the accuracy of the heat polynomials method

4.1. Equalizing calculus

The equalizing calculus cannot be applied to the Trefftz method because the method assumes strict equality of the temperature measured and calculated at all measuring points. In the heat polynomial method measurements T_k, obtained by means of liquid crystal thermography, may be expressed as a sum of unknown accurate measurements $\tilde{T}_k$ and temperature measurements corrections ε_k, that is,

$$\tilde{T}_k = T_k + \varepsilon_k \tag{29}$$

Corrections ε_k are assumed to feature normal distribution with mean value equal to zero and finite variance equal to σ_k^2 [5,36]. σ_k are local temperature measurement errors given by formula (2) and discussed in detail in [17,28,32]. Correction ε_k is determined so as to minimize the Lagrange function:

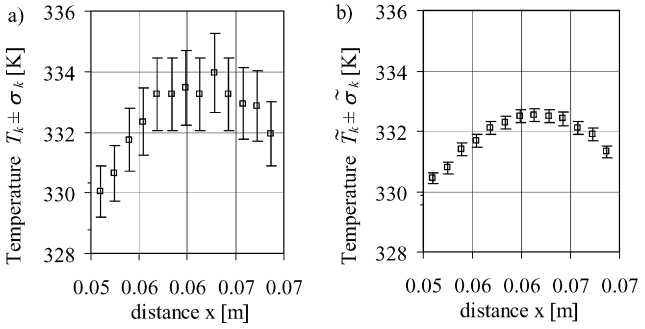

Fig. 11. (a) $T_k \pm \sigma_k$ – temperature and its error distributions in near boiling incipience (for run #12). (b) $\tilde{T}_k \pm \tilde{\sigma}_k$ – smoothed temperature and its error distributions in near boiling incipience (for run #12).

$$\Omega = \sum_{k=1}^{K} \frac{\varepsilon_k^2}{\sigma_k^2} + 2\sum_{k=0}^{K} \omega_k \left(\tilde{T}_F(x_k, \delta_G) - \tilde{T}_k\right) \to \min \tag{30}$$

where $\tilde{T}_F$ is the smoothed foil temperature [5,23]. Additionally, we assume equality between the smoothed temperature $\tilde{T}_F$, and the smoothed measurement of temperature $\tilde{T}_k$:

$$\tilde{T}_F(x_k, \delta_G) - \tilde{T}_k = 0 \tag{31}$$

For the smoothed results – $\tilde{T}_k$, obtained from satisfying conditions (30) and (31), their measurement errors are calculated and denoted as $\tilde{\sigma}_k$, following the procedure described in [5,17]. Fig. 11 presents temperature T_k measurement distributions and temperature $\tilde{T}_k$ smoothed measurement distributions with marked measurement errors σ_k and $\tilde{\sigma}_k$, respectively. As expected, equalizing calculus smoothes the measurement data of temperature $T_k (T_k \to \tilde{T}_k)$ and reduces the errors $\sigma_k (\sigma_k \to \tilde{\sigma}_k)$, Fig. 11. If we know the $\tilde{T}_k$ values, it is possible to calculate new approximations of glass and foil temperatures, and consequently the new heat fluxes and heat transfer coefficients.

4.2. Experimental errors implementation

In the original heat polynomials method, when forming error functionals J_G and J_F (given by formulae (16) and (18) respectively), temperature measurements obtained by means of liquid crystal thermography were assumed to be error-free [5]. In functionals J_G and J_F, the last components $\sum_{k=1}^{K}(T_G(x_k, \delta_G) - T_k)^2$, $\sum_{k=1}^{K}(T_F(x_k, \delta_G) - T_k)^2$ describe how accurately the computed approximations of glass and foil temperatures satisfy the condition (12). In the modified heat polynomials method, taking into consideration temperature measurement errors σ_k, Eq. (2) in functionals J_G and J_F will result in reducing the difference between the calculated approximations and measured temperature values [17,28,32].

Modified are the last components in functionals J_G and J_F (other components in J_G and J_F remain unchanged), which have the following new forms:

$$\text{(a)} \quad \text{for glass: } \sum_{k=1}^{K}\left(\frac{T_G(x_k, \delta_G) - T_k}{\sigma_k}\right)^2$$

$$\text{(b)} \quad \text{for foil: } \sum_{k=1}^{K}\left(\frac{T_F(x_k, \delta_G) - T_k}{\sigma_k}\right)^2 \tag{32}$$

In formulae (32), errors σ_k are weights for individual temperature measurements. The higher the accuracy of the measurement, i.e., the smaller the error, the greater the weight. The described modification of the heat polynomials method improves conditioning of systems of Eqs. (17) and (19) [28].

The introduction of equalizing calculus and modification into the heat polynomials method and their combination increased substantially the accuracy with which the calculated temperatures fulfill boundary conditions, Eqs. (12) and (13); already discussed in [17,27,32]. It also slightly reduced mean relative errors $\Delta q_w/q_w$ and $\Delta\alpha/\alpha$. The smallest mean relative errors were obtained again for the modified heat polynomials method with the use of equalizing calculus. For instance, for run #12, Fig. 5, error $\Delta\alpha/\alpha$ was reduced from 16.45% (for the original heat polynomials method; Table 1) to 15.79% and for run #23 from 15.60% down to 14.74%.

5. General conclusions

Liquid crystal thermography was applied in the discussed studies of boiling heat transfer in minichannels for the identification of two-dimensional temperature fields. This method allowed us to determine two-dimensional temperature distribution on the heating surface, locate the boiling front (boiling incipience), and calculate the local temperature of the heating surface contacting the boiling liquid, local heat flux and the heat transfer coefficient.

Boiling incipience is demonstrated by a sudden decrease in the wall temperature, called "boiling front", caused by appearing vapor bubbles, which behave like heat sinks. A shift of the "boiling front" along the channel length is caused by variation of the volumetric heat flux supplied to the foil. The front is accompanied by the occurrence of nucleation hysteresis. It is characteristic of the boiling of a liquid with a small wetting angle and its appearance is associated with the activation of some nuclei on the heated wall.

It should be emphasized that the main raw data available in the minichannel boiling heat transfer experiment employing thermosensitive liquid crystal technique are the hue distribution along the heating foil and volumetric heat flux, generated inside the foil. Local surface temperature, boiling heat flux and heat transfer coefficient – the most important parameters for boiling process discussion – originate from a data reduction procedure, which requires a solution of the two-dimensional inverse boundary heat conduction problem.

For the reduction of the experimental data obtained from the liquid crystal thermography, we proposed the two-dimensional heat transfer model for the system: flowing liquid – heating foil – liquid crystals – protecting glass. The modified heat polynomials method combined with equalizing calculus was employed to find a numerical solution to the inverse boundary heat conduction problem.

The methodology of error estimation was discussed, focusing on the heating surface temperature measurement carried out with the use of liquid crystal thermography. The known temperature measurement errors were then used in the equalizing calculus in numerical calculations for determining the local heat transfer coefficient. Measurement errors as weights for particular temperature measurements helped to modify the heat polynomials method, which in turn reduced the calculation errors. The proposed new one-dimensional heat transfer model, based on reasonable simplifications, helps to perform fast and simple data reduction.

Acknowledgements

This work was carried out as part of the grant awarded by the Ministry of Science and Higher Education, Poland, no. 3T 10B 015 27.

References

[1] C.N. Ammerman, S.M. You, Enhanced convective boiling of FC-87 in small, rectangular, horizontal channels: heat transfer coefficient and CHF, ASME-HTD 357 (4) (1998) 225–233.

[2] Z.Y. Bao, D.F. Fletcher, B.S. Haynes, Flow boiling heat transfer of Freon R11 and HCFC123 in narrow passages, Int. J. Heat Mass Transfer 43 (2000) 3347–3358.
[3] Z. Bilicki, The relation between the experiment and theory for nucleate forced boiling, in: Proc. 4th World Conf. Experimental Heat Transfer, Fluid Mechanics and Thermodynamics, vol. 2, Brussels, Belgium, 1997, pp. 571–578.
[4] T. Bohdal, Development of bubbly boiling in channel flow, Experimental Heat Transfer 4 (2001) 199–215.
[5] S. Brandt, Data Analysis, Statistical and Computational Methods for Scientists and Engineers, Springer-Verlag, New York, 1999.
[6] Y. Chin, An experimental study on flow boiling in a narrow channel: from convection to nucleate boiling, PhD thesis, Univ. of Houston, Dept. Mech. Eng., Houston, 1997.
[7] Y. Chin, L.C. Witte, D.K. Hollingsworth, Investigation of flow boiling incipience in a narrow rectangular channel using liquid crystal thermography, ASME-HTD 357 (3) (1998) 79–86.
[8] M. Cialkowski, A. Frackowiak, Heat Functions and their Application to Solving Heat Conduction in Mechanical Problems, Publishing House of Poznan, Univ. of Technology, Poznan, Poland, 2000 (in Polish).
[9] M. Cialkowski, S. Futakiewicz, L. Hozejowski, Heat polynomials applied to direct and inverse heat conduction problems, in: Proc. Int. Symp. Trends in Continuum Physics – TRECOP'98, World Scientific, Poznan, Poland, 1998, pp. 79–86.
[10] L. Collatz, The Numerical Treatment of Differential Equations, Springer-Verlag, Berlin, 1966.
[11] V. Dupont, J.R. Thome, Evaporation in microchannels; influence of the channel diameter on heat transfer, in: Proc. 2nd Int. Conf. Microchannels and Minichannels, Rochester, USA, 2004, CD-ICMM2004-2369.
[12] I. Hapke, H. Boye, J. Schmidt, Onset of nucleate boiling in minichannels, Int. J. Thermal Sci. 39 (2000) 505–513.
[13] J.L. Hay, D.K. Hollingsworth, Calibration of micro-encapsulated liquid crystals using hue angle and a dimensionless temperature, Exp. Thermal Fluid Sci. 18 (1998) 251–257.
[14] D.K. Hollingsworth, Application of liquid crystal thermography to flow boiling heat transfer in minichannels, in: Proc. 5th Int. Conf. Boiling Heat Transfer, Montego Bay, Jamaica, 2003, 10 p.
[15] D.K. Hollingsworth, Liquid crystal imaging of flow boiling in minichannels, in: Proc. 2nd Int. Conf. on Microchannels and Minichannels, Rochester, USA, 2004, pp. 57–66.
[16] J.P. Holman, Experimental Methods for Engineers, McGraw-Hill, 1989.
[17] S. Hozejowska, M. Piasecka, M.E. Poniewski, Equalizing calculus in minichannel flow boiling heat transfer calculation, in: Proc. ECI Int. Conf. Heat Transfer and Fluid Flow in Microscale, Castelvecchio Pascoli, Italy, 2005, paper #25.
[18] S.G. Kandlikar, Fundamental issues related to flow boiling in minichannels and microchannels, Exp. Thermal Fluid Sci. 26 (2002) 389–407.
[19] G.M. Lazarek, S.H. Black, Evaporative heat transfer, pressure drop and critical heat flux in a small vertical tube, Int. J. Heat Mass Transfer 25 (1982) 945–960.
[20] Y.M. Lie, F.Q. Su, R.L. Lai, T.F. Lin, Experimental study of evaporation heat transfer characteristics of refrigerants R-134a and R-407C in horizontal small tubes, Int. J. Heat Mass Transfer 49 (2006) 207–218.
[21] J. Orozco, C. Hanson, A study of mixed convection boiling heat transfer in narrow gaps, ASME-HTD 206 (2) (1992) 81–85.
[22] W. Owhaib, C. Martin-Callizo, B. Palm, Evaporative heat transfer in vertical circular minichannels, Applied Thermal Engineering 24 (2004) 1241–1253.
[23] K.S. Park, W.H. Choo, K.H. Bang, Flow boiling heat transfer of R-22 in small diameter horizontal round tubes, in: Proc. 1st Int. Conf. Microchannels and Minichannels, Rochester, USA, 2003, pp. 623–628.
[24] X.F. Peng, H.Y. Hu, B.X. Wang, Boiling nucleation during liquid flow in microchannels, Int. J. Heat Mass Transfer 41 (1998) 101–106.
[25] X.F. Peng, B.X. Wang, Forced convection and flow boiling heat transfer for liquid flowing through microchannels, Int. J. Heat Mass Transfer 36 (1993) 3421–3427.
[26] M. Piasecka, Theoretical and experimental investigations into flow boiling heat transfer in a narrow channel, PhD thesis, Kielce Univ. of Technology, Dept. Mech. Eng., Kielce, 2002 (in Polish).
[27] M. Piasecka, S. Hozejowska, M.E. Poniewski, Experimental evaluation of flow boiling incipience of subcooled fluid in a narrow channel, Int. J. Heat Fluid Flow 25 (2004) 159–172.
[28] M. Piasecka, S. Hozejowska, M.E. Poniewski, Experimental error analysis and heat polynomial method improvement for boiling heat transfer numerical calculations in minichannels, in: Proc. 3rd Int. Conf. Microchannels and Minichannels, Toronto, Canada, 2005, CD-ICMM2005-75142.
[29] M. Piasecka, M.E. Poniewski, Flow boiling incipience in minichannels, in: Proc. 3rd Int. Symp. Two-phase Flow Modeling and Experimentation, Pisa, Italy, 2004, CD-mt-13.
[30] M. Piasecka, M.E. Poniewski, Hysteresis phenomena at the onset of subcooled nucleate flow boiling in microchannels, Heat Transfer Eng. J. 25 (2004) 44–51.
[31] M. Piasecka, M.E. Poniewski, Influence of selected parameters on boiling heat transfer in minichannels, in: Proc. 2nd Int. Conf. Microchannels and Minichannels, Rochester, USA, 2004, pp. 515–522.
[32] M. Piasecka, M.E. Poniewski, S. Hozejowska, L. Hozejowski, Various models and numerical procedures of boiling heat transfer calculations in minichannels, in: Proc. Euromech Colloquium #472 – Microfluidics and Transfer, Grenoble, France, 2005, 4 p.
[33] R. Revelin, J.R. Thome, Experimental investigation of R-134a and R-245fa two-phase flow in microchannels for different flow conditions, in: Proc. ECI Int. Conf. Heat Transfer and Fluid Flow in Microscale, Castelvecchio Pascoli, Italy, 2005, CD-No. 14.
[34] E. Sobierska, K. Chmiel, R. Kulenovic, R. Mertz, Experimental investigation on flow boiling in a vertical narrow channel, in: Proc. 3rd Int. Conf. Microchannels and Minichannels, Toronto, Canada, 2005, CD-ICMM2005-75124.
[35] S. Su, S. Huang, X. Wang, Study of boiling incipience and heat transfer enhancement in forced flow through narrow channels, Int. J. Multiphase Flow 31 (2005) 253–260.
[36] J. Szargut, Equalizing Calculus in Heat Engineering, Ossolineum, Katowice, Poland, 1984 (in Polish).
[37] L. Tadrist, Review of two-phase flow instabilities in narrow spaces, in: Proc. ECI Int. Conf. Heat Transfer and Fluid Flow in Microscale, Castelvecchio Pascoli, Italy, 2005, CD-No. 25.
[38] J.R. Thome, Boiling in microchannels: a review of experiment and theory, Int. J. Heat Fluid Flow 25 (2004) 128–139.
[39] Y. Tian, X.D. Wang, X.F. Peng, Characteristics of earlier nucleation for boiling in microchannels, in: Proc. 2nd Int. Conf. Microchannels and Minichannels, Rochester, USA, 2004, CD-ICMM2004-2386.
[40] L. Wang, M. Chen, M. Groll, Experimental study on flow boiling heat transfer in mini-tube, in: Proc. 3rd Int. Conf. Microchannels and Minichannels, Toronto, Canada, 2005, CD-ICMM2005-75026.
[41] B.X. Wang, X.F. Peng, Boiling characteristics of subcooled liquid flowing through microchannels, in: Proc. 6th Int. Symp. Transport Phenomena in Thermal Engineering, vol. 1, Seoul, Korea, 1993, pp. 417–421.
[42] L. Wojtan, R. Revellin, J.R. Thome, Investigation of critical heat flux in single, uniformly heated microchannels, in: Proc. ECI Int. Conf. Heat Transfer and Fluid Flow in Microscale, Castelvecchio Pascoli, Italy, 2005, CD-No. 6.
[43] Y.Y. Yan, T.F. Lin, Evaporation heat transfer and pressure drop of refrigerant R-134a in a small pipe, Int. J. Heat Mass Transfer 41 (1998) 4183–4194.
[44] Y. Yang, Y. Fujita, Flow boiling heat transfer and flow pattern in rectangular channel of mini-gap, in: Proc. 2nd Int. Conf. Microchannels and Minichannels, Rochester, USA, 2004, CD-ICMM2004-2383.
[45] T. Yen, N. Kasagi, Y. Suzuki, Forced convective boiling heat transfer in microtubes at low mass and high heat fluxes, Int. J. Multiphase Flow 29 (2003) 1771–1792.